CHEMISTRY OF MATERIALS

ARTICLE

pubs.acs.org/cm

Aminophenylnitronylnitroxides: Highly Networked Hydrogen-Bond Assembly in Organic Radical Materials

Safo Aboaku,[||,†] Armando Paduan-Filho,[‡] Valdir Bindilatti,[‡] Nei Fernandes Oliveira, Jr.,[‡] John A. Schlueter,[§] and Paul M. Lahti*[,†]

[†]Department of Chemistry, University of Massachusetts, Amherst, Massachusetts 01003, United States

[‡]Instituto de Física, Universidade de São Paulo, São Paulo, SP 05315-970, Brazil

[§]Materials Science Division, Argonne National Laboratory, Argonne, Illinois 60439, United States

Supporting Information

ABSTRACT: 2-(*Meta*-aminophenyl)-4,4,5,5-tetramethyl-4,5-dihydro-*1H*-imidazole-3-oxide-1-oxyl (mAPN) and 2-(*para*-aminophenyl)-4,4,5,5-tetramethyl-4,5-dihydro-*1H*-imidazole-3-oxide-1-oxyl (pAPN) were synthesized and subjected to magnetostructural analysis. Both form extended hydrogen bonding networks involving both amino NH bonds to radical spin-density bearing nitronylnitroxide NO groups. Their crystallographic assembly motifs and magnetic exchange properties are compared to those of *tert*-butoxylcarbonyl (BOC) and amide derivatives having only one NH bond. The conversion of pAPN to acid salt derivatives gives a solid that is essentially diamagnetic, although dissolution of the solid shows the radical spin units to be preserved.

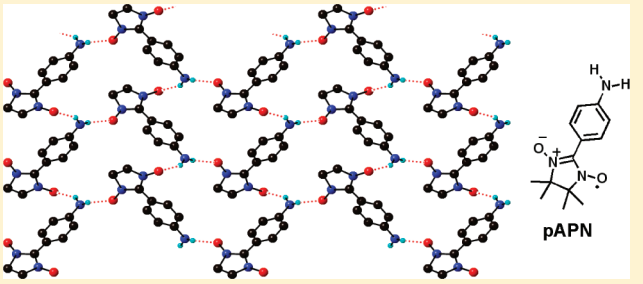

KEYWORDS: molecular magnetism, hydrogen bonding, nitronylnitroxides, radicals

INTRODUCTION

The field of molecule-based magnetism frequently utilizes molecular assembly to achieve some degree of predictable crystal packing. Purely organic, metal-free magnetic materials are particularly dependent on assembly, because interspin exchange interactions are only significant across short distances for upper-row elements. Bringing specific portions of spin-bearing molecules into proximity can frequently be done using hydrogen bonding interactions. The attachment of various functional groups to unpaired spin carriers such as aminoxyl, nitronylnitroxide, and verdazyl radicals can induce intermolecular exchange interactions ranging from simple pairing to three-dimensionally ordered ferromagnetism in the solid state. Dependable prediction of magnetism remains an elusive challenge for organic radical-based solids, in part, because sure prediction of crystal packing also remains elusive. However, the past 10−15 years of work by various groups has shown a number of useful correlations between specific intermolecular solid state arrangements and qualitative magnetic exchange behaviors.[1]

Phenolic groups have been used with some frequency for assembling radicals, especially nitronylnitroxides (Chart 1). Sugawara and co-workers carried out studies of HQNN,[2] which has two allotropes, the α-form of which forms paired hydrogen-bonding chains and orders as an organic ferromagnet at T_c = 0.5 K. Veciana and co-workers have carried out studies on 2HOPhNN, 3HOPhNN, 4HOPhNN, and NNCatH2,[3] which form various hydrogen bonded motifs including dimers, chains, and 2-D sheets, at least one of which[3d] appears to form a quasi-2D ferromagnetic phase. Matsushita et al. have studied RSNN, which shows hydrogen-bond assisted spin pairing.[4] Taylor and Lahti investigated[5] the effect of sterically inhibiting hydrogen bonding by the phenolic OH through *tert*-butylation in HOBu2PhNN, and they found that 1-D zigzag OH to ON hydrogen bonding arrays formed, albeit with changes in hydrogen bonding geometry relative to 4HOPhNN as a result of steric constraints caused by the *tert*-butyl groups. These various studies show that phenolic hydrogen bonds can assemble organic spin units with significant intermolecular exchange interactions between radicals.

We aimed to replace the OH group of phenolic nitronylnitroxides with an NH_2 group to induce extended hydrogen-bonding motifs similar to those found in phenolic nitronylnitroxides, but with enhanced networking because NH_2 can form two hydrogen bonds with the major spin bearing aminoxyl N−O· groups, whereas OH can only form one (Scheme 1) unless bifurcated interactions occur. Of course, other (albeit weaker) hydrogen bond like interactions can occur, such as methyl CH to aminoxyl N−O· contacts exemplified in Scheme 1 for the phenolic compounds. However, in hopes of realizing higher dimensionality networks of the stronger hydrogen bonds involving NH and NH_2 groups, we targeted the syntheses of 2-(*meta*-aminophenyl)-4,4,5,5-tetramethyl-4,5-dihydro-*1H*-imidazole-3-oxide-1-oxyl (mAPN) and

Received: August 5, 2011
Revised: September 15, 2011
Published: October 06, 2011

Chart 1

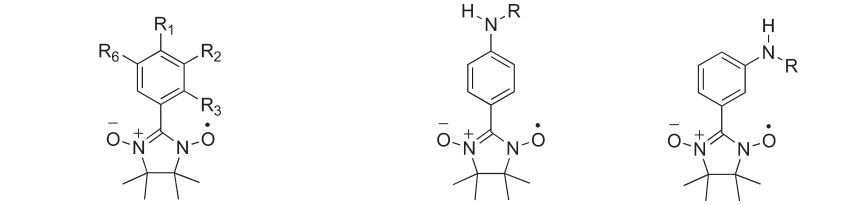

HQNN, $R_3 = R_5 = OH, R_1 = R_2 = H$
2HOPhNN, $R_2 = OH, R_1 = R_2 = R_6 = H$
3HOPhNN, $R_2 = OH, R_1 = R_3 = R_6 = H$
4HOPhNN, $R_1 = OH, R_2 = R_3 = R_6 = H$
NNCatH$_2$, $R_1 = R_2 = OH, R_6 = H$
RSNN, $R_2 = R_6 = OH, R_1 = R_3 = H$
HOBu$_2$PhNN, $R_1 = OH, R_2 = R_6 = C(CH_3)_3$

pAPN, R = H
pAcPN, R = acetyl
pBocPN, R = CO(O-*t*-Bu)

mAPN, R = H
mAcPN, R = acetyl
mBocPN, R = CO(O-*t*-Bu)

Scheme 1. Comparing Hydrogen Bonding Possibilities for OH and NH$_2$ Containing Nitronylnitroxides

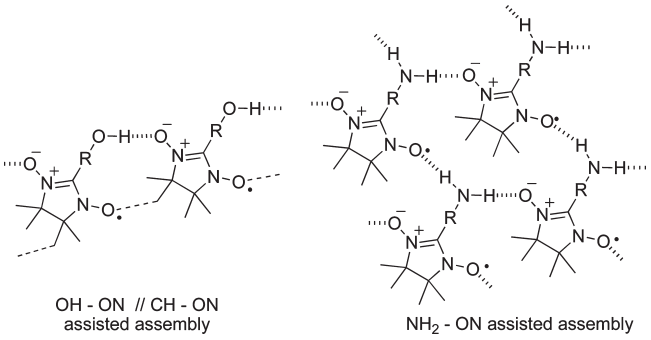

2-(*para*-aminophenyl)-4,4,5,5-tetramethyl-4,5-dihydro-*1H*-imidazole-3-oxide-1-oxyl (pAPN). In this article, we report the preparation, properties, and magnetostructural analyses of mAPN and pAPN, with comparisons to corresponding acetamide and *tert*-butoxycarbonyl (BOC) derivatives that have only one NH unit available for hydrogen bonding. We also describe preliminary studies of protonated ammonium cations of pAPN derived by treating the neutral radical with mineral acids.

EXPERIMENTAL SECTION

General Methods. 2,3-Bis(hydroxylamino)-2,3-dimethylbutane monosulfate was made by the method of Ovcharenko, Fokin, and Rey.[6] Full details for the syntheses shown in Scheme 2 are given in the Supporting Information, including intermediates meta-acetamidobenzyl alcohol,[7] meta-acetamidobenzaldehyde,[8] and 2-(para-(*tert*-butoxycarbonyl)-aminobenzaldehyde.[9]

2-(*Meta*-acetamidophenyl)-4,4,5,5-tetramethyl-4,5-dihydro-*1H*-imidazole-3-oxide-1-oxyl (mAcPN). Dark blue crystals, mp 197−199 °C. FTIR (KBr, cm^{-1}): 3262 (N−H), 2987 (methyl C−H), 1665 (C═O). MS (FAB): found m/z = 291.0, $C_{15}H_{20}N_3O_3$ requires m/z = 290.3. EPR (9.651 GHz): g = 2.0069, a(N) = 7.42 gauss (2N).

2-(*Meta*-(*tert*-butoxylcarbonyl)aminophenyl)-4,4,5,5-tetramethyl-4,5-dihydro-*1H*-imidazole-3-oxide-1-oxyl (mBocPN). Dark blue crystals, mp 165−167 °C. FTIR (KBr, cm^{-1}): 3328 (NH), 2980 (methyl C−H), 1726 (C═O). MS(FAB): found m/z 348.2, $C_{18}H_{26}N_3O_4$ requires m/z 348.4. EPR (9.652 GHz): g = 2.0065, a(N) = 7.41 gauss (2N).

2-(*Meta*-aminophenyl)-4,4,5,5-tetramethyl-4,5-dihydro-*1H*-imidazole-3-oxide-1-oxyl (mAPN). Blue-black crystals, mp 150−152 °C. FTIR (KBr, cm^{-1}): 3392, 3328, 3232 (NH), 2925 (methyl C−H). MS(FAB): found m/z 248.14, $C_{13}H_{18}N_3O_2$ requires m/z 248.30. EPR (9.651 GHz): g = 2.0063, a(N) = 7.35 gauss (2N).

2-(*Para*-acetamidophenyl)-4,4,5,5-tetramethyl-4,5-dihydro-*1-H*-imidazole-3-oxide-1-oxyl (pAcPN). Blue-black solid, mp 204−205 °C. FTIR (KBr, cm^{-1}): 3341 (NH), 2992 (methyl C−H), 1707 (C═O). EPR (9.650 GHz): g = 2.0068, a(N) = 7.49 gauss (2N). Anal. for $C_{15}H_{20}N_3O_3$ requires C, 62.05; H, 6.94; N, 14.47. Found: C, 61.90; H, 6.91; N, 14.45.

2-(*Para*-(*tert*-butoxylcarbonyl)aminophenyl)-4,4,5,5-tetramethyl-4,5-dihydro-*1H*-imidazole-3-oxide-1-oxyl (pBocPN). Blue-black solid, mp 215−218 °C. FTIR (KBr, cm^{-1}): 3340 (NH), 2980 (methyl C−H) 1728 (C═O). EPR (9.652 GHz): g = 2.0068, a(N) = 7.47 gauss (2N). Anal. for $C_{18}H_{26}N_3O_4$ requires C, 62.05; H, 7.52; N, 12.06. Found: C, 62.03; H, 7.55; N, 12.04.

2-(*Para*-aminophenyl)-4,4,5,5-tetramethyl-4,5-dihydro-*1H*-imidazole-3-oxide-1-oxyl (pAPN). Blue-green prisms, mp 147−150 °C. FTIR (KBr, cm^{-1}): 3446, 3334, 3214 (NH), 2926 (methyl C−H). EPR (9.644 GHz): g = 2.0062, a(N) = 7.87 gauss (2N). Analysis for $C_{13}H_{18}N_3O_2$ requires: C, 62.87; H, 7.32; N, 16.92. Found: C, 63.27; H, 7.41; N, 16.21.

2-(*Para*-aminophenyl)-4,4,5,5-tetramethyl-4,5-dihydro-*1H*-imidazole-3-oxide-1-oxyl Hydrochloric Acid Salt (pAPN·HCl). Neutral radical pAPN (0.20 g, 0.80 mmol) was stirred in 30 mL of dichloromethane at room temperature under nitrogen, as 2 mL of 1 M HCl in ether was added slowly by syringe. The mixture was stirred under nitrogen for 20 min. The mixture was filtered, and the solid residue was washed with dichloromethane to yield 66 mg (29%) of product pAPN·HCl as a dark greenish solid. FTIR (KBr, cm^{-1}): 2120−3320 (br, NH). MS(FAB[+]): $C_{13}H_{19}N_3O_2^+$ requires m/z = 249.15, found 250.16 (M+H). The absorption spectra of pAPN·HCl are concentration dependent. UV−vis (MeOH): (13.8 μM: 320 nm); (55 μM: 325); (220 μM: 354 nm, 418 nm); (878 μM: 440 nm). The EPR of the neat solid showed only a very weak peak at $g \sim 2$. The EPR spin counts comparing methanol solutions of pAPN and pAPN·HCl showed ~30% of spins retained in the salt. Solutions of pAPN·HCl showed loss of color and EPR signal within 24 h. Adding KOH to a green methanol solution of pAPN·HCl regenerates the blue color of neutral pAPN.

2-(*Para*-aminophenyl)-4,4,5,5-tetramethyl-4,5-dihydro-*1H*-imidazole-3-oxide-1-oxyl Hydrofluoroboric Acid Salt (pAPN·HBF$_4$). Neutral radical pAPN (0.100 g, 0.403 mmol) was stirred in 15 mL of methanol at room temperature under nitrogen, as 400 μL of tetrafluoroboric acid solution (48 wt % HBF_4 in water) was added slowly by syringe. The mixture was stirred under nitrogen for 2 h, then evaporated under reduced pressure to give a liquid with some

dx.doi.org/10.1021/cm202303q |*Chem. Mater.* 2011, 23, 4844–4856

precipitate. This residue was further cooled in the freezer. The remaining liquid was pipetted away, and the remaining solid dried under vacuum for 4 h. This solid was washed with dichloromethane and dried in air to yield 61 mg (45%) of pAPN·HBF_4 as a brown solid. FTIR (KBr, cm^{-1}): 2570−3320 (br, NH), 1056 (B−F). MS(FAB[+]): $C_{13}H_{19}N_3O_2^+$ requires m/z = 249.15, found m/z = 250.1 (M + H); [−]-mode found m/z = 86.98 (BF_4^-). pAPN·HBF_4 absorption spectra are concentration dependent. UV−vis (MeOH): (14 μM: 322 nm, 417 nm); (55.8 μM: 320 nm, 413 nm); (223 μM: 437 nm); (893 μM: 461 nm). The EPR of the neat solid pAPN·HBF_4 showed only a very weak peak at $g \sim 2$. EPR spin counts comparing methanol solutions of pAPN and pAPN·HBF_4 showed 64% of spins retained in the salt. Solutions of the radical salt showed the same instability in air and color changes upon addition of base that were observed for pAPN·HCl.

Crystallographic Measurements. Room temperature single crystal X-ray diffraction measurements were carried out for mAcPN, mBocPN, mAPN and pAPN at the University of Massachusetts Amherst X-ray Structural Characterization Facility on a Bruker-Nonius KappaCCD instrument (setup supported by NSF CHE-9974648 and the University of Massachusetts Chemistry Department), using molybdenum source λ = 0.71073 Å radiation. Structures were solved by direct methods using SHELXTL.[10] The 15 K structure of pAPN was determined at the ChemMatCARS (Sector 15) beamline at the Advanced Photon Source. The crystallography for pAcPN and pBocPN has been previously reported[11] by Aboaku and Lahti; various details of these are used for comparison in this full report. New structure data have been deposited with the Cambridge Crystallographic Data Centre. Further details are given in the Supporting Information CIF files.

Magnetic Measurements. Dc magnetic susceptibility (χ) measurements at 1.8−300 K were carried out at the University of Massachusetts Amherst Nanomagnetics Facility (NSF CTS-0116498) with a Quantum Design MPMS-7 magnetometer using crushed, polycrystalline samples placed in gelatin capsules and held in place by a plug of cotton. Temperature independent corrections to susceptibility were made by the extrapolation of the uncorrected high temperature χT data. pAPN was also analyzed at 0.5−4 K, using a custom built apparatus[12] at Universidade de São Paulo.

Computations. Computational modeling of spin densities used fixed crystallographic geometries of the monoradicals at the UB3LYP[13]/EPR-III level of theory with the Gaussian[14] program. Estimates of the exchange interactions were made using computations with crystallographically derived dyad and triad geometries. For intermolecular exchange modeling, hybrid density functional UB97D computations using Grimme's dispersion corrected functional (for better treatment of nonbonded interactions)[15] with the 6-31G+(d) basis set were carried out using the crystallographic geometries of close-contact dyads: methyl groups on the radical units were replaced by hydrogen atoms in most cases. For singlet−triplet (S-T) state energy splitting, the singlet state was modeled by a broken symmetry unrestricted UB3LYP wave function, which gives a highly spin-contaminated "state" with corresponding[16] uncertainties. Yamaguchi's scheme[17,18] was used to adjust for the spin contamination in the state energies by eq 1:

$$\Delta E_{T-S} = \frac{E_S - E_T}{\langle S^2_{HS}\rangle - \langle S^2_{LS}\rangle} \quad (1)$$

where $\langle S^2\rangle$ is the spin-squared expectation value from the triplet (T) and singlet (S) multiplicity computations and $\Delta E > 0$ for a triplet the ground state. Zero point energy corrections are not included.

RESULTS AND DISCUSSION

Synthesis. Our initial synthetic plan for mAPN and pAPN was to convert *meta*- and *para*-aminobenzyl alcohols to amides, oxidize to corresponding aldehydes, condense with 2,3-bis(hydroxylamino)-2,3-dimethylbutane, oxidize to the corresponding nitronylnitroxides, and hydrolyze the amide groups to the desired amines. However, various efforts to convert amidophenyl nitronylnitroxides mAcPN and pAcPN to aminophenyl nitronylnitroxides were not satisfactory. The sequences shown in Scheme 2 gave much better yields of mAPN and pAPN, as well as providing boc-carbamate-functionalized radicals mBocPN and pBocPN. We have given a preliminary report[11] of the syntheses and magnetostructural studies of pAcPN and pBocPN.

All of the radicals were deep blue solids that appear to be indefinitely stable in air at room temperature. Single crystals of each were subjected to X-ray diffraction analysis, the results of which are detailed in Table 1 and in the Supporting Information. ORTEP[19] diagrams for each are shown in Figure 1. Solutions of each showed the typical 1:3:5:3:1 pentet electron paramagnetic resonance (EPR) spectra expected for nitronylnitroxides, arising from hyperfine coupling of the two equivalent nitrogen atoms.

Crystallographic Packing Motifs that Influence Exchange between Nitronylnitroxides. Scheme 3 shows some basic intermolecular parameters that strongly affect exchange between N−O groups. Stronger exchange, in general, is favored by smaller distances $r_{O/O'}$ and $r_{O/N'}$, which bring sites of strong spin density into close proximity. However, considering only the distances between spin sites (dipolar approximation) is inadequate because π-type orbital overlap and the resulting interaction are orientation dependent, as in the strong overlap between π-spin orbitals of an antiparallel stacked arrangement of NO groups ($\varphi < 90°$) that leads to AFM exchange.[20] Strong exchange is favored when $\varphi = 45-90°$, because this forces the NO groups into closer proximity. Where loci of the three atoms attached to the nitrogen of an NO radical site form a plane, the parameter ζ should be about zero to allow the NO spin orbital sites to point toward one another as needed for AFM exchange. If $\zeta \sim 90°$, then the NO spin units are nearly orthogonal to one another, a situation that promotes FM exchange. Finally, the pseudodihedral angle ω in Scheme 3 should be about 90° to minimize "side-slipping" that decreases spin orbital overlap. The interplay between these parameters is complex and subtle, but each affects whether there is strong spin orbital overlap between NO units that favors AFM exchange, or not. To summarize, in Scheme 3 the following promote AFM exchange: smaller distances $r_{O/O'}$ and $r_{O/N'}$, $\varphi = 45-90°$, $\zeta \sim 0°$, and $\omega \sim 90°$. In various cases in the discussion below, we will note to how these parameters correlate with exchange in Table 2.

Novoa and co-workers[21] have used a somewhat larger set of intermolecular contact definitions (some analogous to those in Scheme 3) in a sophisticated and compelling study relating crystallographically identified, pairwise exchange interactions to the experimental exchange and magnetic behavior of several nitronylnitroxides. They showed that the subtle interplay among so many variables renders extremely difficult a confident assignment of overall magnetic behavior to specific exchange interactions coming from specific contacts, unless one of the contacts is very strongly dominant. Also, at low temperatures, the crystal lattice volume and intermolecular contact distances (or even geometries) will change somewhat by comparison to room temperature structures. The computational dyad exchange interactions given below should therefore be viewed as an effort to identify qualitative tendencies for exchange: large differences in exchange behavior between geometric contacts are qualitatively meaningful, while small differences should be considered too close to call.

Scheme 2. Syntheses of Nitronylnitroxide Radicals

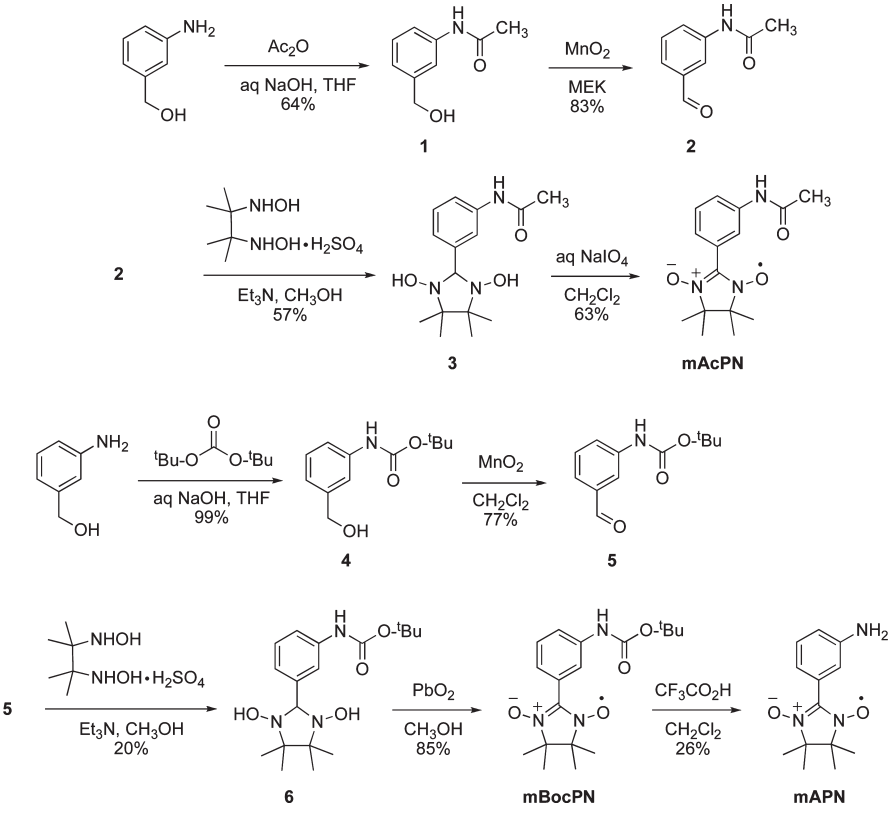

***N*-Functionalized Aminophenyl Nitronylnitroxides: Limited Hydrogen Bonding Cases.** Acetyl substituted mAcPN forms hydrogen-bonded chains along the crystallographic *c*-axis involving only the amide units (Figure 2, labeled *c*), with pendant radical groups on alternating sides of the chain. Nitronylnitroxide N−O···O−N contacts form chains perpendicular to the hydrogen-bonded chains, along the crystallographic *b*-axis (labeled *b* in Figure 2), with $r_{O/O'}$ contact r(O10···O11′) = 3.83 Å at 293 K. Because φ = ∠N9−O10···O11′−(N7) = 143° and angle ω = ∠C8−N9−O10···O11′−(N7) = 123°, the overlap of singly occupied molecular orbitals (SOMOs) here is poor. Magnetic measurements for mAcPN (Figure 3) confirm this, showing essentially paramagnetic behavior. From a Curie−Weiss plot of $1/\chi$ versus T, the Curie constant C = 0.368 emu·K/Oe·mol—in good agreement with the expected value for $S = {}^1/_2$ radical spin carriers—with a Weiss constant of only θ = (−)0.3 K.

By comparison, mBocPN forms hydrogen-bonded chains between BOC N−H donor groups and nitronylnitroxide N−O acceptor groups (Figure 4, labeled b_1, dashed lines). Overall, the nitronylnitroxides are linked by chain contacts along the crystallographic *b*-axis (Figure 4, labeled b_2). These chain contacts between N−O groups provide a possible AFM exchange pathway between sites of large spin density, as shown in Scheme 4, with $r_{O/O'}$ contact b_2 having r(N9)−O10···O11′−(N) = 3.97 Å and φ = ∠N9−O10···O11′−(N7) = 108.2°. The oxygen ends of the NO groups are not well aligned for SOMO−SOMO overlap, with an obtuse angle φ and interplane angle ζ = 43°, which is much larger than in mAcPN; ζ should be nearly zero for best overlap.

The $1/\chi$ versus T plot for mBocPN yields a Curie constant of C = 0.374 emu·K/Oe·mol and a modest Weiss constant of θ = (−)0.8 K (Figure 5). Computations show nearly zero spin density at the N−H group for mBocPN, so the $r_{O/O'}$ contact r[(N9)−O10···O11′−(N7)] (labeled b_2 in Figure 4) is presumably the main contributor to the modest AFM exchange here, with no exchange coupling across the hydrogen bond. The modest exchange is in accord with the poor overlap of the SOMOs in this geometry.

Because of our preliminary report of results for pAcPN and pBocPN,[11] we only briefly summarize these results for comparison. Both form cyclic dyads with the amide N−H groups hydrogen-bonded to N−O groups, as shown in Figure 6 (contacts *a*). UB3LYP/EPR-III computations show virtually no spin density on the amide groups; so, hydrogen bonding should not provide an electronic pathway for exchange interactions. However, in pAcPN, the N−O groups that are not involved in hydrogen bonding form antiparallel stacked pairs between hydrogen-bonded dyads, with $r_{O/O'}$ contact r[(N4)−O15···O15′−(N4)] = 4.103 Å, and φ = ∠N4−O15···O15′−(N4) = 73.3° across contact *b* in the upper part of Figure 6. However, the aminoxyl O15 also is nearly equidistant from the neighboring N4′ atom (Table 2, $r_{O/N'}$) and the attached C11′ atom. The O15···N4′ contact would typically be expected to favor AFM exchange, but the O15···C11′ contact to favor FM exchange. This is a case where a small shift of N−O groups relative to one another could influence the exchange significantly, for example, by lattice contraction during cooling for magnetic measurements.

Radical pAcPN exhibits significant AFM exchange, as shown by the downturn in its χ versus T susceptibility plot (Figure 7).

dx.doi.org/10.1021/cm202303q |*Chem. Mater.* 2011, 23, 4844–4856

Table 1. Crystallographic Data and Structure Refinement for mAcPN, mBocPN, mAPN, pAcPN, pBocPN, and pAPN

	mAcPN	mBocPN	mAPN
temp. (K)	293	293	293
chemical formula	$C_{15}H_{20}N_3O_3$	$C_{18}H_{26}N_3O_4$	$C_{13}H_{18}N_3O_2$
chemical formula wt	290.34	348.42	248.3
wavelength (Å)	0.71073	0.71073	0.71073
crystal system, space group	orthorhombic, $Pna2_1$	orthorhombic, $Pbca$	monoclinic, $P2_1/c$
a, b, c (Å)	19.9092(5)	13.922(5)	7.738(5)
	7.7405(1)	11.778(5)	19.085(5)
	9.5638(2)	24.558(5)	19.085(5)
α, β, γ (deg)	90.0	90.0	90.0
	90.0	90.0	102.262(5)
	90.0	90.0	90.0
V (Å^3)	1473.85(5)	4027(2)	1320.2(12)
Z	4	8	4
D_{calc} (Mg/m^3)	1.309	1.15	1.249
$F(000)$	620	1496	532
μ (mm^{-1})	0.093	0.082	0.086
R_{int}	0.0352	0.0840	0.0425
completeness to 2θ	1.00	0.992	0.995
N_{ref}, param.	2720, 237	3530, 250	3129, 220
goodness of fit on F^2	1.051	1.071	1.023
$\Delta\rho_{max}$, $\Delta\rho_{min}$ (e − Å^{-3})	0.148, −0.158	0.535, −0.293	0.175, −0.153
R_1, wR_2 ($I > 2\sigma(I)$)	0.0363, 0.0924 (2204)	0.084, 0.2337 (2530)	0.0425, 0.1043 (2109)
R_1, wR_2 (all)	0.0495, 0.0991 (2720)	0.1065, 0.2643 (3530)	0.0716, 0.1193 (3129)

	pAcPN[a]	pBocPN[b]	pAPN	pAPN
temp. (K)	293	293	293	15
chemical formula	$C_{15}H_{20}N_3O_3$	$C_{18}H_{26}N_3O_4$	$C_{13}H_{18}N_3O_2$	$C_{13}H_{18}N_3O_2$
chemical formula wt	290.34	348.42	248.3	248.3
wavelength (Å)	0.71073	0.71073	0.71073	0.44280
cell setting, space group	monoclinic, $P2_1/c$	monoclinic, $P2_1/n$	orthorhombic, $Pbca$	orthorhombic, $Pbca$
a, b, c (Å)	11.2200(2)	12.0543(3)	13.7796(7)	13.7284(6)
	12.4690(2)	9.9704(4)	12.3236(6)	12.2673(6)
	11.3440(2)	16.3448(7)	16.0651(4)	16.0254(8)
α, β, γ (deg)	90.0	90.0	90.0	90.0
	103.289(1)	105.579(3)	90.0	90.0
	90.0	90.0	90.0	90.0
V (Å^3)	1544.55(5)	1892.25(12)	2728.1(2)	2698.8(2)
Z	4	4	8	8
D_{calc} (g/cm^3)	1.249	1.223	1.209	1.222
$F(000)$	620	748	1064	1064
μ (mm^{-1})	0.088	0.087	0.083	0.053
R_{int}	0.0461	0.0427	0.0334	0.0689
completeness to 2θ	0.997	0.993	0.997	0.997
N_{ref}, param.	2823, 271	4305, 330	3113, 202	3505, 172
goodness of fit on F^2	0.986	1.00	1.035	1.033
$\Delta\rho_{max}$, $\Delta\rho_{min}$ (e − Å^{-3})	0.224, −0.202	0.147, −0.283	0.184, −0.17	0.358, −0.329
R_1, wR_2 ($I > 2\sigma(I)$)	0.0461, 0.1374 (2256)	0.049, 0.1058 (2446)	0.0598, 0.1436 (1818)	0.0622, 0.1756 (2562)
$R_{\sigma 1}$, wR_2 (all)	0.0578, 0.1521 (2823)	0.1087, 0.1295 (4305)	0.1108, 0.1713 (3113)	0.0799, 0.1975 (3505)

[a] From CSD TICXAF, CCDC Deposition No. 619977 and ref 11. [b] From CSD TICWUY, CCDC Deposition No. 619976 and ref 11.

dx.doi.org/10.1021/cm202303q |*Chem. Mater.* 2011, 23, 4844–4856

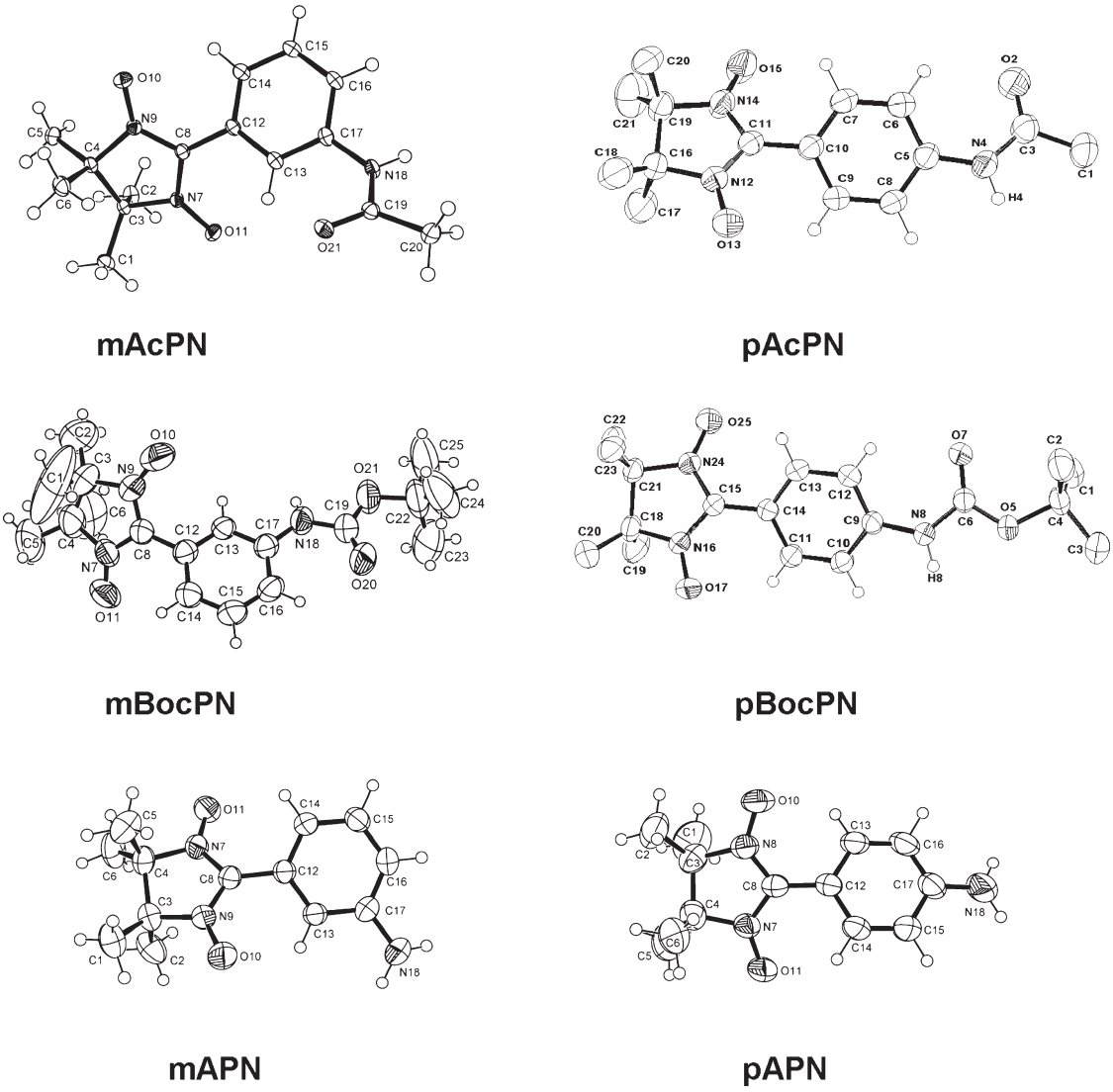

Figure 1. ORTEP diagrams showing thermal ellipsoids at 50% probability. Some hydrogen atoms have been omitted in structures for ease of viewing.

Using a singlet−triplet spin pairing Hamiltonian $H = -2JS_1S_2$ and eq 2:[22]

$$\chi = \left[\frac{2Ng^2\beta^2}{3k(T-\theta_{MF})}\frac{3}{3+\exp(2J/kT)}\right]\cdot(1-F) + (F)\cdot 0.375\frac{1}{T} \quad (2)$$

where the singlet−triplet energy splitting is $2J/k$, using a mean field correction of θ_{MF}, where F is a correction for paramagnetic sites in the lattice, and other terms have the usual meanings, we found g = 1.998, $2J/k$ = (−)5.0 K, and θ_{MF} = (−)0.86 K, assuming no paramagnetic impurities (F = 0). These are in close agreement with those from our preliminary report for pAcPN.[11] Using the room temperature crystal structure for pAcPN, the computationally estimated dyad singlet−triplet energy splitting is $2J/k$ = (−)2.4 K at the UB97D/6-31+G(d) level and (+)1.2 K at the UB3LYP/6-31G* level. The qualitatively different computed results possibly arise as a result of the competition of the FM and AFM contacts at different levels of theory.

By comparison to pAcPN, pBocPN has no close contacts between large nitronylnitroxide spin density sites in its crystal lattice. It also lacks close contacts of its NO groups with other sites of spin density that are large enough to yield indirect exchange pathways. The lack of intermolecular exchange pathways is consistent with the essentially paramagnetic, isolated spin behavior of pBocPN. Its $1/\chi$ versus T plot (Figure 8) fitted over the full temperature range yields a Curie constant of 0.372 emu·K/Oe·mol, in excellent agreement with the value expected for $S = {}^1/_2$ radicals; the Weiss constant derived by linear fit over the full temperature range is only θ = (−)0.2 K and that for the data with T > 100 K only θ = (+)0.5 K. The full temperature Weiss constant is more consistent with an observed small downturn in χT versus T (not shown), indicating very small AFM exchange in the lattice.

Aminophenyl Nitronylnitroxides: Networked Hydrogen Bonding Cases. As we hoped, when choosing amino groups as hydrogen bonding units, each mAPN −N18(H_2) amino group hydrogen bonds with nitronylnitroxide N7−O11 groups from two different molecules, contacts *a* and *b* in Figure 9. Overall, a 3-D network results involving these hydrogen bonds, as well as

dx.doi.org/10.1021/cm202303q |*Chem. Mater.* 2011, 23, 4844–4856

N9−O10 to nitronylnitroxide C5 methyl group contacts (not shown). The *a* hydrogen bond has $r(N18(H)_2\cdots O11'a)$ = 3.111 Å, with ∠N18···O11′−N7′*a* = 127.8°; the *b* hydrogen bond has $r(N18(H)_2\cdots O11''a)$ = 3.168 Å, with ∠N18···O11″−N7″*b* = 119.1°. The N9−O10 nitronylnitroxide groups are not hydrogen bonded with $-NH_2$. Instead, they form N−O···O−N antiparallel-stacked dyads related by inversion symmetry (contact *c* in Figure 9), an $r_{O/O'}$ type contact with r(N9−O10···O10′N9′) = 3.537 Å and φ = ∠N9−O10···O10′(N)′ = 76°. The acute angle of φ with relatively small $r_{O/O'}$ and $r_{O/N'}$ (Table 2) provides significant SOMO−SOMO overlap between the nitronylnitroxide units, with significant AFM exchange interaction expected.

A plot of $1/\chi$ versus T for mAPN yields a Curie constant of C = 0.368 emu·K/Oe·mol and a large, AFM Weiss constant of θ = (−)36.2 K by the linear fitting of the T > 150 K data: the plot deviates strongly from linearity below 100 K (Figure 10a). The χ versus T data show a maximum at 40−50 K (Figure 10b), characteristic of AFM exchange. At 1.8 K, magnetization versus field experiments saturate at a small value (Supporting Information) attributable to some paramagnetic sites in the lattice—most magnetic moment is lost at low temperature, consistent with spin pairing. A nonlinear least squares fit to the χ versus T data, using the singlet−triplet susceptibility eq 1 with fitting of J/k and $S = {}^1/_2$ paramagnetic fraction F (same Hamiltonian as eq 1), yields $2J/k$ = (−)83.0 K, with F = 6%, using a fixed g = 1.9. If the mean field correction of eq 1 is included using g = 1.98 from the Curie−Weiss plot, the fit is significantly better, with $2J/k$ = (−)62.6 K, θ_{MF} = (−)17.9 K, and F = 6%. The fitted curves are shown in Figure 10b. With or without the mean-field correction, the magnetic data show fairly strong AFM interactions, which the crystallographic analysis attribute to the antiparallel N−O···O−N stack. The hydrogen bonding in mAPN thus forms a scaffold that holds the radical groups in proximity to produce this interaction. The computationally estimated dyad singlet−triplet energy splitting across the antiparallel N−O···O−N stack is $\Delta E(S \rightarrow T) = 2J/k$ = (−)30.5 K at the UB97D/6-31+G(d) level, and (−)8.6 K at the UB3LYP/6-31G* level.

The crystallography of radical pAPN has significant differences from that of mAPN. A private communication to the Cambridge Structural Database of the crystal structure *only* for pAPN gives[23] essentially the same structure as that found in the present work. Similarly to mAPN, pAPN forms an intricate network of hydrogen bonds. However, in pAPN every $-NH_2$ group not only bridges two nitronylnitroxide N−O units by close contacts but also *every* nitronylnitroxide group is hydrogen bonded to two $-NH_2$ groups. Figure 11 shows the contacts schematically. The hydrogen bonded network forms 2-D corrugated sheets lying in the crystallographic *bc*-plane (shown in the Supporting Information). Figure 11 shows the closest $r_{O/O'}$ type contact in pAPN (contact *c*) across an inversion center with r([N2]−O2···O2′−[N2′]) = 3.60 Å but with a very obtuse φ = ∠N2−O2···O2′−(N) = 136°. These contacts occur along

Scheme 3. Geometric Close Contact Parameters for Inter-Radical Exchange

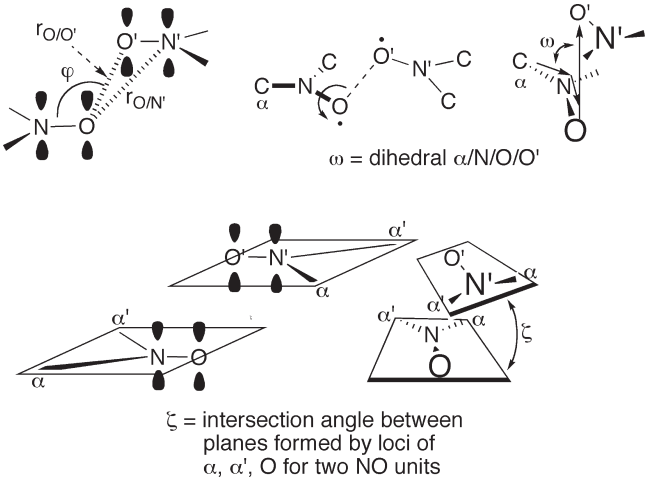

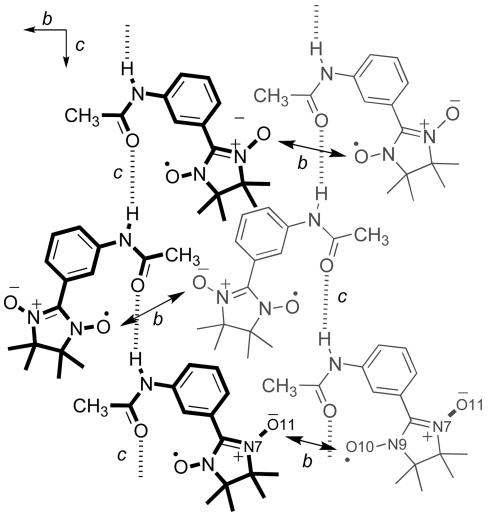

Figure 2. Important hydrogen bonding and N−O···O−N intermolecular close contacts in mAcPN.

Table 2. Experimental and Computer Modeled Exchange[a]

	exptl exchange[b]	computed NO···ON dyad exchange, $2J/k$ UB3LYP, [UB97D][c]	$\langle S^2_{HS}\rangle$,$\langle S^2_{LS}\rangle$[d]	$r_{O/O'}$ (Å)	$r_{O/N'}$ (Å)	φ (deg)	ζ (deg)	ω (deg)
mAcPN	θ = (−) 0.3 K	(−)0.25 K, [(+) 0.35 K]	2.11, 1.11 [2.03, 1.03]	3.83	4.91[e], 4.57[f]	118[g], 143[h]	10	48[i], 127[j]
mBOC	θ = (−) 0.8 K	(not computed)		3.97	4.08[k], 4.53[l]	108[m], 86[n]	43	122[o], 85[p]
mAPN	$2J/k$ = (−) 83.0 K	(−)8.6 K, [(−) 30.5 K]	2.12, 1.12 [2.03, 1.03]	3.54	3.46	76	0	74.5
pAcPN	$2J/k$ = (−) 5.0 K	(+)0.60 K, [(−) 4.8 K]	2.11, 1.11 [2.03, 1.03]	4.10	3.93	73	9	77
pAPN	θ = (−) 3.4 K	(−)0.2 K, [(+) 1.4 K]	2.11, 1.11 [2.03, 1.03]	3.60	4.62	136	0	43

[a] Room temperature NO···ON intermolecular dyad contact parameters from definitions in Scheme 3. Double entries have angles calculated starting from the NO group that corresponds to the $r_{O/N'}$ distance (from NO to the nearby N′). [b] Negative values for AFM exchange. [c] Computed gaps using eq 1; UB97D values in brackets, [ ]. [d] UB97D values in brackets, [ ]. [e] N9···O11. [f] N7···O10. [g] N7−O11···O10. [h] N9−O10···O11. [i] C5−N7−O11···O10. [j] C3−N9−O10···O11. [k] N7···O10. [l] N9···O11. [m] N9−O10···O11. [n] N7−O11···O10. [o] C3−N9−O10···O11. [p] C4−N7−O11···O10.

dx.doi.org/10.1021/cm202303q |*Chem. Mater.* 2011, 23, 4844–4856

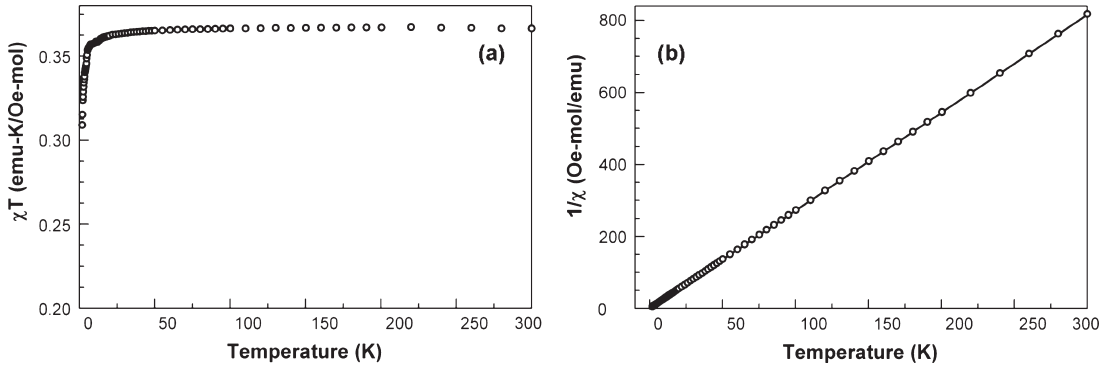

Figure 3. Paramagnetic susceptibility (χ) for mAcPN as χT vs T (chart a) and $1/\chi$ vs T (chart b) plots, at 1000 Oe external field.

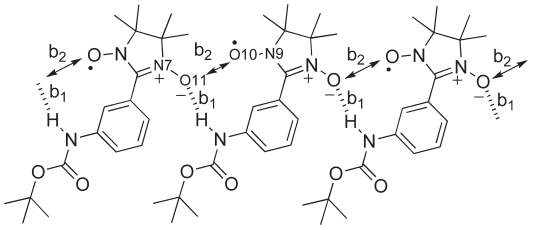

Figure 4. Important hydrogen bonding and N−O···O−N intermolecular close contacts in mBocPN.

the crystallographic *a*-axis, across boundaries between the hydrogen-bonded 2-D sheets. Because of the obtuse φ parameter (Table 2), the N−O groups are oriented nearly "head-on" with very little SOMO−SOMO overlap possible, although they are close enough for some dipole−dipole exchange. This N−O···O−N contact *c* also involves close N−O···H−C(aryl) contacts involving the phenyl ring C−H that is ortho to the radical group connection, as shown in Figure 11. With so many atoms held in close proximity and some of them having large spin densities, it is not straightforward to analyze qualitatively what exchange is expected to occur.

The computationally estimated dyad singlet−triplet energy splitting across the pAPN N−O···O−N contact was $2J/k$ = (+)1.5 K at the UB97D/6-31+G(d) level; at the UB3LYP/6-31G* level it is $2J/k$ = (−)0.2−0.3 K. The much smaller interaction than in the case of mAPN is presumably due to the head-on orientation of the contact, rather than parallel overlapping geometry. The small computed interaction suggests that low temperature changes in crystal contacts could change exchange behavior relative to higher temperatures. The following analysis of intermolecular contacts is thus only indicative of qualitative trends and only if exchange contacts do not change significantly.

The largest exchange component is expected from the $r_{O/O'}$ N2−O2···O2′−N2′ contact, as a result of the large spin densities involved. However, the direct N−H···O−N contacts might provide indirect exchange pathways through the small spin density on N−H. The *a* N3−H3A···O1−N1 contact has its N−H bond pointing almost directly toward an N−O lone pair, and this will not provide close overlap of spin density on the NH hydrogen with the nitronylnitroxide spin orbital. However, the *b* contact N3−H3B···O2−N2 has its N−H bond pointing almost directly at the oxygen lobe of an N−O SOMO. Notably, r(N3[H3A]···O1) for the *a* contact is much shorter, 2.936(3) Å versus the *b* contact of r(N3[H3B]···O2) = 3.402(4) Å. The

Scheme 4. Hydrogen Bonding Contacts and Qualitative Spin Density Distributions in mBocPN

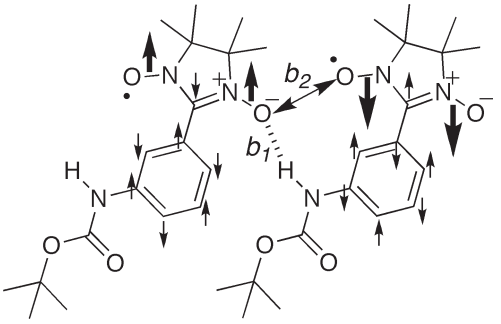

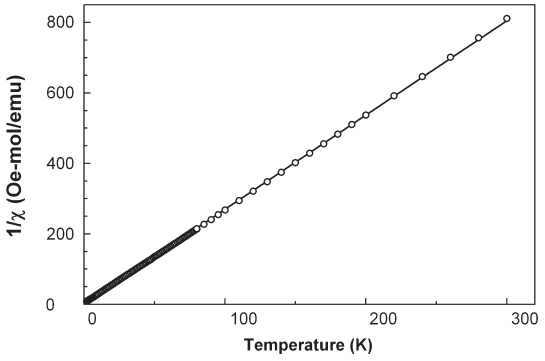

Figure 5. Reciprocal paramagnetic susceptibility $1/\chi$ vs T plot for mBocPN, at 1000 Oe external field.

b contact is longer because H3B is pointed toward an N−O SOMO, not toward a lone pair as in a classic hydrogen bond.

The *a* N−H···O−N contact gives near-orthogonality of the hydrogen s-orbital and the O−N SOMO, while the *b* N−H···O−N contact gives good overlap of the analogous orbitals; these are shown between molecules Y and Z in Scheme 5. The two types of hydrogen bonds could give qualitatively different exchange interactions, as shown in Scheme 5 using the spin densities computed for an isolated pAPN molecule (see Supporting Information). Taylor and Lahti noted[5] an analogous difference in comparing expected exchange in phenolic nitronylnitroxides having direct O−H···O−N contacts with different geometries. Using the

dx.doi.org/10.1021/cm202303q |*Chem. Mater.* 2011, 23, 4844–4856

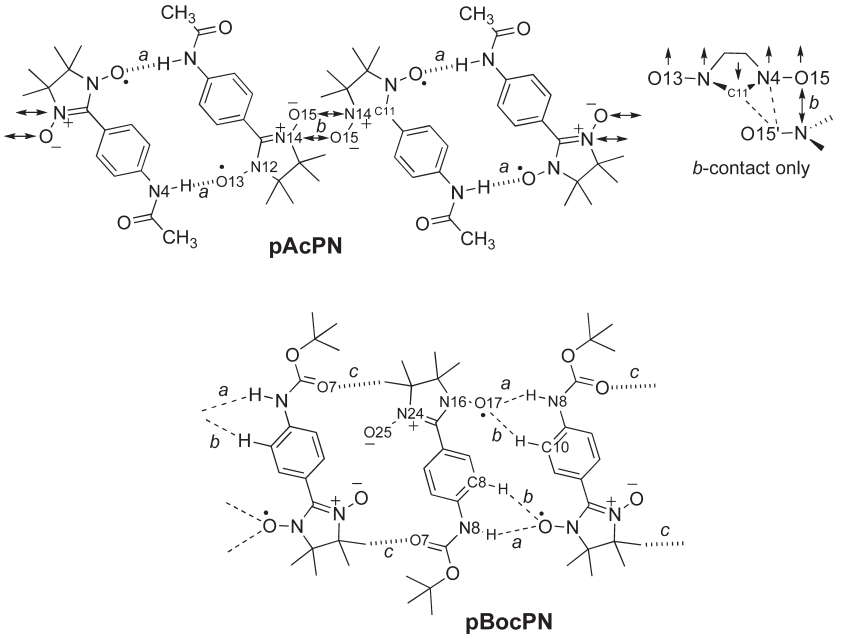

Figure 6. Hydrogen bonding and N−O···O−N intermolecular close contacts in pAcPN (upper) and pBocPN (lower).

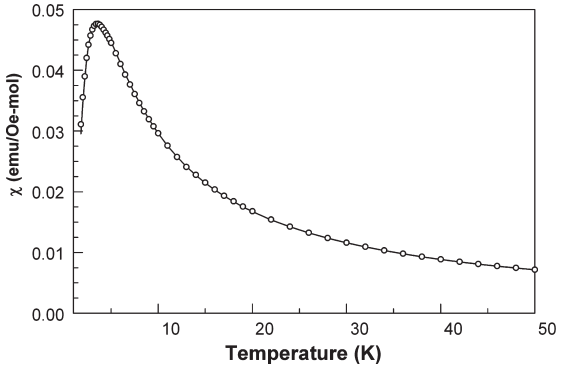

Figure 7. Paramagnetic susceptibility χ vs T plot for pAcPN, at 1000 Oe external field.

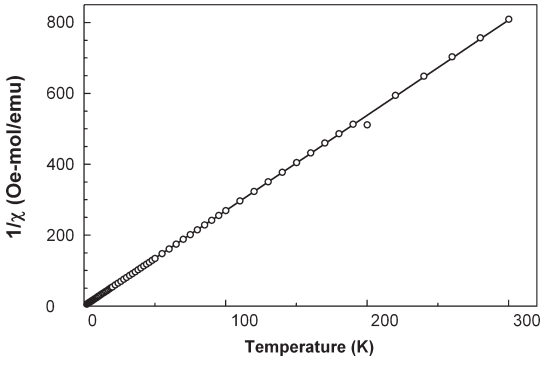

Figure 8. Reciprocal paramagnetic susceptibility $1/\chi$ vs T plot for pBocPN, at 1000 Oe external field.

crystallographic geometries used to formulate the qualitative descriptions of Scheme 5, the *a* N−H···O−N contact is computed to have $2J/k$ = (+)0.15 K and the *b* N−H···O−N contact has $2J/k$ = (−)0.03 K, both at the UB97D/6-31+G(d) level. At the

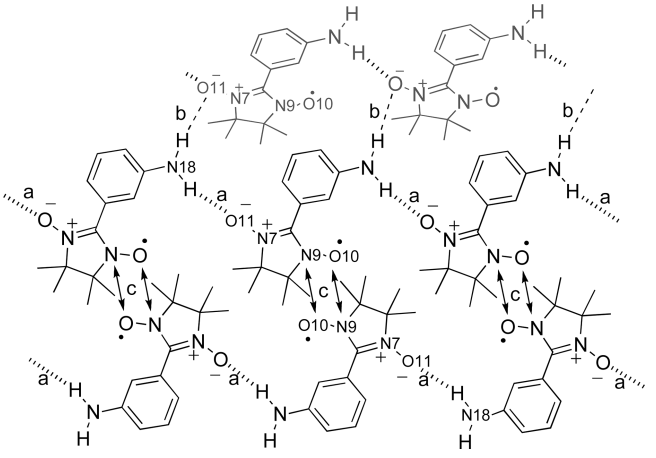

Figure 9. Important hydrogen bonding and N−O···O−N intermolecular close contacts in mAPN in the crystallographic *ac*-plane.

UB3LYP/6-31G* level, $2J_a/k$ = (+)0.03 K and $2J_b/k$ = (−)0.25 K. The computed numbers are so small that it is hard to depend strongly qualitative dyad exchange model of the *a* and *b* contacts in Scheme 5. Also, N−H bond lengths and positions from the crystallographic analysis are subject to the uncertainties of estimating the hydrogen atom positions.

The experimental magnetic behavior for pAPN is shown in Figure 12. The χ versus T data lie below the paramagnetic Curie curve, indicating AFM exchange. The higher temperature region of the $1/\chi$ versus T plot yields a Curie constant of 0.363 emu·K/Oe·mol and an extrapolated Weiss constant of θ = (−)3.4 K but with a change of slope at about 5 K; the 2−5 K region extrapolates to θ = (−)0.3 K. The antiferromagnetic interactions in higher temperature region are also seen in the χT versus T plot, which decreases significantly in the range 50−3 K. However, the decrease levels out at 2−3 K, so we also investigated the susceptibility behavior in the range 0.5−3.6 K.

dx.doi.org/10.1021/cm202303q |*Chem. Mater.* 2011, 23, 4844–4856

Interestingly, χT versus T increases again after minimizing at about 2 K, indicating competing exchange pathways in pAPN. A $1/\chi$ versus T plot of the 0.6−3.6 K data yields a small positive Weiss constant of (+)0.26 K, with a Curie constant of only about 0.2 emu·K/Oe·mol. The Curie constant is also consistent with the molar magnetization versus field data at 1.8 K, which appear to approach saturation at about $^2/_3$ the value expected for 1 mol of $S = {}^1/_2$ radicals. The behavior suggests multiple exchange pathways are present, although there is only one crystallographic form of pAPN in the lattice. As the temperature decreases, a dominant AFM exchange interaction gives the downturn of χT versus T, yielding the significant negative Weiss constant of the higher temperature region of the $1/\chi$ versus T plot. Presumably, the relatively close AFM contact c, (N2)−O2···O2′−(N2′), between molecules W and X in Scheme 5, dominates exchange in the higher temperature region. At lower temperatures, small FM interactions—possibly through the hydrogen bonding network—cause the χT versus T plot to rise again.

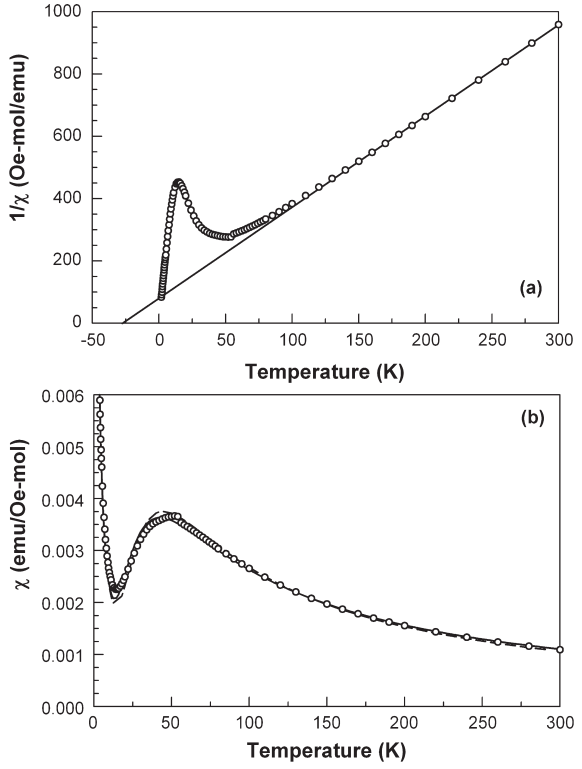

Figure 10. Paramagnetic susceptibility data plots for mAPN, as $1/\chi$ vs T (a), with linear fitted line from data where $T > 150$ K, and χ vs T (b), with a broken line for the fitted curve to eq 1 without mean field and a solid line for the curve with the mean field included. All data obtained using 1000 Oe external field.

Scheme 5. Hydrogen Bonding Contacts and Qualitative Spin Density Distributions in pAPN

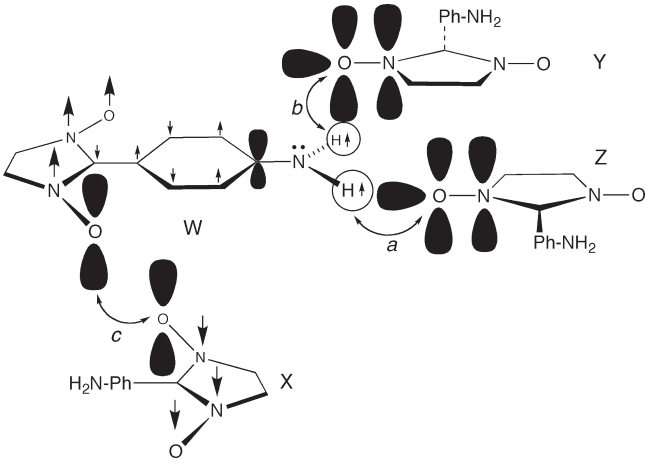

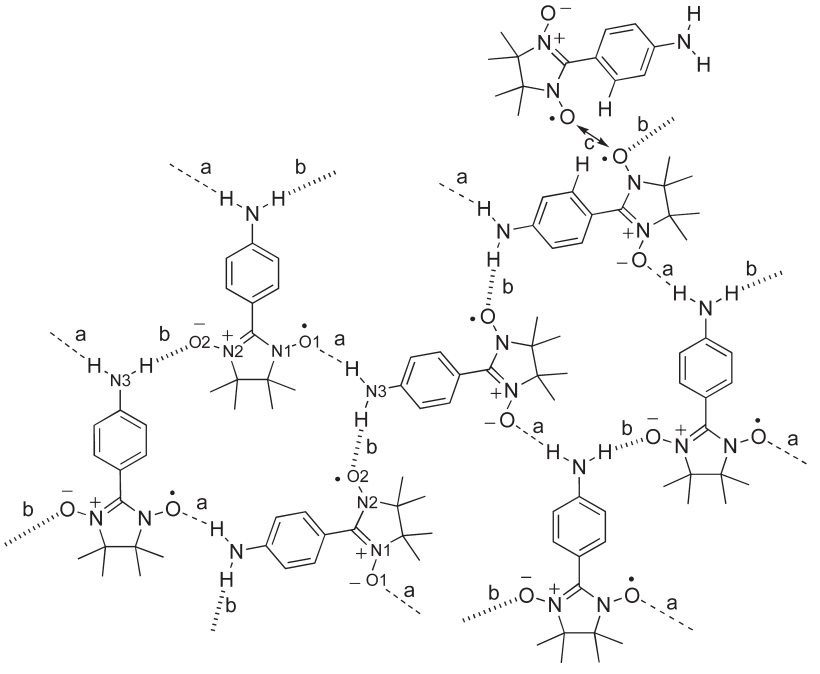

Figure 11. Important hydrogen bonding and N−O···O−N intermolecular close contacts in pAPN in the crystallographic *bc*-plane.

dx.doi.org/10.1021/cm202303q |*Chem. Mater.* 2011, 23, 4844–4856

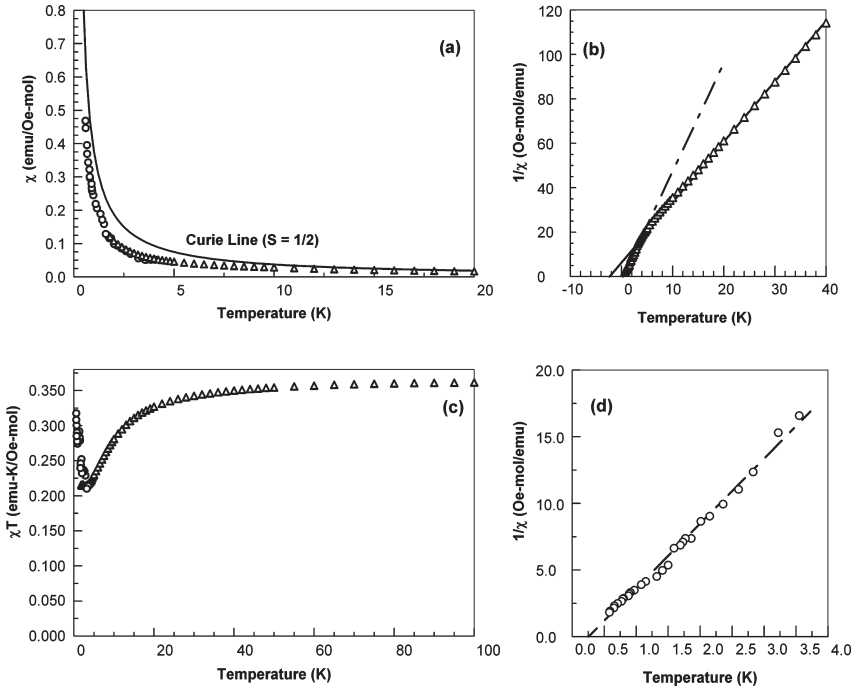

Figure 12. For pAPN: (a) paramagnetic susceptibility χ vs T plot showing a noninteracting spins Curie line; (b) Curie−Weiss $1/\chi$ vs T plot showing linear fits to data at higher (solid line) and lower (broken line) temperature regions; (c) χT vs T plot; and (d) low temperature $1/\chi$ vs T plot showing linear fit to data. Data obtained at $T \geq 1.8$ K at 1000 Oe are shown as open triangles in chart a; data obtained at 0.6 K < T < 4 K at zero field, by ac-susceptibility (modulation field 5 Oe, modulation frequency 155 Hz) are shown as open circles.

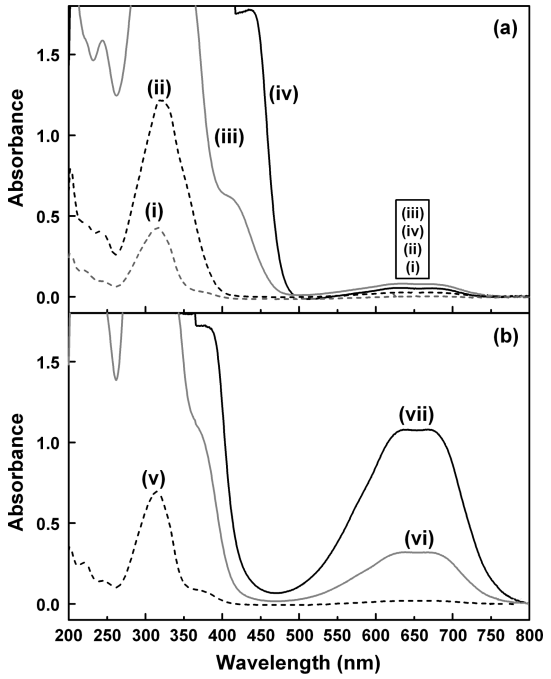

Figure 13. UV−vis spectra in methanol for (a) pAPN·HCl at 878 μM (i), 220 μM (ii), 55 μM (iii), and 13.8 μM (iv); (b) pAPN at 805 μM (v), 201 μM (vi), and 12.6 μM (vii). The letters in the chart a inset box at long wavelength show the descending order of the lines at that point.

We considered the possibility that the network of contacts in pAPN changes as temperature decreases, changing the exchange behavior. However, the pAPN crystal structure at 15 K remains remarkably similar to the room temperature structure. As shown in Table 1, the crystallographic axes contract by only 0.3−0.5%; the largest absolute change is 0.056 Å along the b-axis. The unit cell volume contracts by only 1.1%. A crystal packing similarity analysis[24] of the structures at both temperatures gives a root mean square (rms) difference of only 0.03. The high resistance to contraction for pAPN upon cooling is attributable to the highly networked array of hydrogen bonds, which rigidify the lattice packing by comparison to what would be expected for more localized interactions. It seems unlikely that cooling below 15 K would lead to additional major changes to the crystal lattice.

The complexity of the contact network in Figure 11 makes it challenging to identify any structure feature as the cause of the lower temperature magnetic behavior. As Novoa and co-workers have pointed out,[21] it is very risky to attribute magnetic behavior to any one or limited number of intermolecular contacts in an organic molecular solid, unless the contact creates an exchange interaction that greatly dominates. That is not the case here. As a result, one must be satisfied to note that competing, small exchange effects seem to be present in pAPN.

Aminophenyl Nitronylnitroxide Acid Salts. The Coulombic forces in ionic solids can produce crystallization motifs and exchange effects in acid salts that are quite different from those in corresponding neutral solids. Therefore, pAPN was treated with HBF_4/methanol or HCl in diethyl ether to yield salts pAPN·HBF_4 and pAPN·HCl. Interestingly, the salts showed only very weak EPR spectra as neat solids, but strong 1:3:5:3:1 pentet spectra with $a_N = 7.8$ (HBF_4 salt) and 8.2 gauss (HCl salt) when dissolved in methanol. Unfortunately, solutions of the radical salts decomposed completely within 24−48 h; so, we could not obtain diffraction quality crystals of either. Ullman proposed that nitronylnitroxides disproportionate to nonradical forms upon exposure to acid;[25] such a process may decompose pAPN·HBF_4 and pAPN·HCl in solution. The salts were much

dx.doi.org/10.1021/cm202303q |*Chem. Mater.* 2011, 23, 4844–4856

more stable as solids, producing strong EPR spectra when dissolved after months of storage under ambient conditions. Green-colored solutions of either salt in methanol turn azure blue when treated with KOH. The green color is regenerated upon addition of acid to basic solutions (see Supporting Information). The color changes can be cycled multiple times, so long as the salt solution does not stand for more than a few hours.

Consistent with their lack of strong EPR signals as neat solids, pAPN·HBF_4 and pAPN·HCl samples exhibited little or no paramagnetic susceptibility. The EPR and colorimetric experiments show that the nitronylnitroxide groups remain present in the solids. Apparently there is very strong AFM exchange between radical sites, $J/k \ll (-)300$ K. FTIR spectra show strong, broad bands over 2100−3200 cm^{-1}, consistent with the strong hydrogen bonding of N−H groups in an ionic salt. Without the crystal packing information, one can only speculate about what structural features give the strong spin pairing. Hydrogen bonding must bring the radical groups into unusually close proximity to one another, in a geometry having strong overlap of their spin orbitals for strong AFM exchange.

Although we lack crystallographic data for pAPN·HBF_4 and pAPN·HCl, their solution UV−vis spectra clearly show significant inter-radical aggregation. At about 10 μM concentrations in methanol, the spectra of the free amine and the salts are quite similar, save that the salt has a much-decreased molar absorptivity of its long wavelength nitronylnitroxide absorption at 650 nm. This band may be due to the small amount of free amine in equilibrium with the ammonium salt. At concentrations >200 μM, the ammonium salts exhibit a new, shoulder band at 420 nm, not seen at any concentration of the free amine. The comparative behavior of pAPN and pAPN·HCl is shown in Figure 13, and it indicates significant aggregation of the aminium salt.

Conclusion. Aminophenyl nitronylnitroxides, having two N−H donor sites for hydrogen bonds, form more extensive hydrogen bonding in their N−H crystal lattices than similar compounds having only one N−H or O−H donor site available. For most of the systems, the strongest magnetic exchange interactions are attributable to direct intermolecular contacts having good spin orbital overlap between high spin density nitronylnitroxide sites, typically involving N−O units. Only pAPN shows indications that N−H hydrogen bonding to the radical units may play a direct electronic exchange role in the magnetic behavior. The use of versatile amino groups in these radicals offers promise for further structure−property modification, as exemplified by conversion of pAPN to ammonium salts. However, it seems likely that strategies to raise the critical magnetic ordering temperatures of pure organic radicals (especially for those based solely on elements of the first two rows of the periodic table) will require designs in which directional molecular assembly moieties such as hydrogen bonds can also bear significant spin density on the hydrogen bond donors and acceptors. Doing this would improve prospects for multidimensional exchange interactions to be propagated throughout the molecular material.

■ ASSOCIATED CONTENT

Ⓢ Supporting Information. Crystallographic CIF summaries; figure of 2-D sheet packing in pAPN; Mecury[24] format files of extended hydrogen bonding in mAPN and pAPN; pH-variable color picture of pAPN solutions; infrared spectra of all compounds and the ammonium salts; magnetization versus field plots for all radicals in this study; archive information for computational results reported in this article. This material is available free of charge via the Internet at http://pubs.acs.org.

■ AUTHOR INFORMATION

Corresponding Author
*lahti@chem.umass.edu.

Present Addresses
[‖]Department of Chemistry, University of Mississippi, University, Mississippi 38677.

■ ACKNOWLEDGMENT

This work was supported by the U.S. National Science Foundation (CHE-0415716 [S.A. and P.M.L.], CHE-0809791 [P.M.L.]; synthesis, characterization of all molecules). We thank Dr. A. Chandrasekaran and Dr. P. Khalifah for assistance with crystallographic analyses carried out at the University of Massachusetts. A.P.F., V.B., and N.F.O. thank the Fundação de Ampara á Pesquisa do Estado de São Paulo, Brazil (FAPESP-07/50968-0) for support to carry out the low temperature magnetic study of pAPN. Use of the Advanced Photon Source was supported by the U.S. Department of Energy, Office of Science, Office of Basic Energy Sciences, under Contract No. DE-AC02-06CH11357. ChemMatCARS Sector 15 is principally supported by the National Science Foundation/Department of Energy under Grant No. NSF/CHE-0822838.

■ REFERENCES

(1) (a) Miller, J. S., Gatteschi, D., Eds.; *Chem. Soc. Rev.*, **2011**, *40*, 3053−3368. (b) *Magnetism: Molecules to Materials*; Miller, J. S., Drillon, M., Eds.; Wiley-VCH: Weinheim, Germany, 2001−2005; Vols. 1−5. (c) Kahn, O. *Molecular Magnetism*; VCH: New York, 1993. (c) *Molecular Magnetism: New Magnetic Materials*; Itoh, K, Kinoshita, M, Eds.; Gordon and Breach, Kodansha Ltd.: Tokyo, Japan, 2000. (d) *Magnetic Properties of Organic Materials*; Lahti, P. M., Ed.; Marcel-Dekker: New York, 1999. (e) *Carbon-Based Magnetism: An Overview of the Magnetism of Metal-Free Carbon-Based Compounds and Materials*; Makarova, T., Palacio, F., Eds.; Elsevier: Amsterdam, Netherlands, 2006. (f) Fovira, C., Veciana, J., Eds.; *Crystal. Eng. Comm.* **2009**, *11*, 2017−2212.

(2) (a) Sugawara, T.; Matsushita, M. M.; Izuoka, A.; Wada, N.; Takeda, N.; Ishikawa, M. *Chem. Commun.* **1994**, 1723–4. (b) Matsushita, M. M.; Izuoka, A.; Sugawara, T. *Mol. Cryst. Liq. Cryst. Sci. Technol., Sect. A* **1996**, *279*, 139–144. (c) Matsushita, M. M.; Izuoka, A.; Sugawara, T.; Kobayashi, T.; Wada, N.; Takeda, N.; Ishikawa, M. *J. Am. Chem. Soc.* **1997**, *119*, 4369–4379.

(3) (a) Garcia-Munoz, J. L.; Cirujeda, J.; Veciana, J.; Cox, S. F. J. *Chem. Phys. Lett.* **1998**, *293*, 160–166. (b) Veciana, J.; Cirujeda, J.; Rovira, C.; Vidal-Gancedo, J. *Adv. Mater.* **1995**, *7*, 221–225. (c) Cirujeda, J.; Mas, M.; Molins, E.; Lanfranc de Panthou, F.; Laugier, J.; Park, J. G.; Paulsen, C.; Rey, P.; Rovira, C.; Veciana, J. *Chem. Commun.* **1995**, 709–710. (d) Cirujeda, J.; Hernandez-Gasio, E.; Rovira, C.; Stanger, J.-L.; Turek, P.; Veciana, J. *J. Mater. Chem.* **1995**, *5*, 243–52. (e) Heise, H.; Koehler, F. H.; Mota, F.; Novoa, J. J.; Veciana, J. *J. Am. Chem. Soc.* **1999**, *121*, 9659–9667. (f) Cirujeda, J.; Vidal-Gancedo, J.; Juergens, O.; Mota, F.; Novoa, J. J.; Rovira, C.; Veciana, J. *J. Am. Chem. Soc.* **2000**, *122*, 11393–1140. (g) Cirujeda, J.; Ochando, L. E.; Amigo, J. M.; Rovira, C.; Rius, J.; Veciana, J. *Angew. Chem., Int. Ed. Engl.* **1995**, *34*, 55–57.

(4) Matsushita, M. M.; Izuoka, A.; Sugawara, T.; Kobayashi, T.; Wada, N.; Takeda, N.; Ishikawa, M. *J. Am. Chem. Soc.* **1997**, *119*, 4369–4379.

(5) Taylor, P.; Lahti, P. M. *Chem. Commun.* **2004**, 2686–2688.

(6) Ovcharenko, V.; Fokin, S.; Rey, P. *Mol. Cryst. Liq. Cryst. Sci. Technol., Sect. A* **1999**, *334*, 109.
(7) Grice, R.; Owen, L. N. *J. Chem. Soc.* **1963**, 1947–1954.
(8) Friedlaender, P.; Fritsch, R. *Monatsh. Chem.* **1903**, *24*, 1–12.
(9) Rai, R.; Katzellenbogen, J. *J. Med. Chem.* **1992**, *35*, 4150–4159.
(10) Sheldrick, G. M. *SHELXTL97*, Program for the Refinement of Crystal Structures; University of Göttingen: Germany.
(11) Aboaku, S.; Lahti, P. M. *Polyhedron* **2007**, *26*, 1959–1964.
(12) Oliveira, N. F., Jr.; Paduan-Filho, A.; Salinas, S. R.; Becerra, C. C. *Phys. Rev. B* **1978**, *18*, 6165.
(13) (a) Lee, C.; Yang, W.; Parr, R. G. *Phys. Rev. B* **1988**, *37*, 785. (b) Becke, A. D. *J. Chem. Phys.* **1993**, *98*, 5648. (c) Stephens, P. J.; Devlin, F. J.; Chabalowski, C. F.; Frisch, M. J. *J. Phys. Chem.* **1994**, *98*, 11623.
(14) Frisch, M. J.; et al. *Gaussian 03*, B03 ed.; Gaussian, Inc.: Pittsburgh, PA, 2003. The full citiation is given in the Supporting Information.
(15) Grimme, S. *J. Comput. Chem.* **2006**, *27*, 1787–1799.
(16) Davidson, E. R. *Int. J. Quantum Chem.* **1998**, *69*, 241–245.
(17) Yamaguchi, K.; Fukui, H.; Fueno, T. *Chem. Lett.* **1986**, 625–628.
(18) Yamaguchi, K. *Chem. Phys. Lett.* **1988**, *149*, 537–542.
(19) Program ORTEP3:Farrugia, L. J. *J. Appl. Crystallogr.* **1997**, *30*, 565.
(20) Cf. Yamaguchi, K.; Kawakami, T.; Oda, A.; Yoshioka, Y. In *Magnetic Properties of Organic Materials*; Lahti, P. M., Ed.; Marcel Dekker: New York, NY, 1999; pp 403−425.
(21) Deumal, M.; Ciujeda, J.; Veciana, J.; Novoa, J. J. *Chem.—Eur. J.* **1999**, *5*, 1631–1542.
(22) Bleaney, B.; Bowers, K. D. *Proc. R. Soc. London, Ser. A* **1952**, 214.
(23) Wagner, B.; Gompper, R.; Polborn, K. CCDC Deposition #192763, CSD Code MUKKUY, as a private communication; 2002.
(24) Similarity analysis was carried out using the program Mercury, version 2.3, build RC4, from the Cambridge Crystallographic Data Centre:Macrae, C. F.; Bruno, I. J.; Chisholm, J. A.; Edgington, P. R.; McCabe, P.; Pidcock, E.; Rodriguez-Monge, L.; Taylor, R.; van de Streek, J.; Wood, P. A. *J. Appl. Crystallogr.* **2008**, *41*, 466–470.
(25) Ullman, E. F.; Osiecki, J. H.; Boocock, D. G. B.; Darcy, R. *J. Am. Chem. Soc.* **1972**, *94*, 7049–7059.